Carbon 167 (2020) 140–147

Contents lists available at ScienceDirect

Carbon

journal homepage: www.elsevier.com/locate/carbon

Shear-induced diamondization of multilayer graphene structures: A computational study

Shiddartha Paul [a], Kasra Momeni [a, b, c, *], Valery I. Levitas [d]

[a] Department of Mechanical Engineering, Louisiana Tech University, Ruston, LA, 71272, USA
[b] Institute for Micromanufacturing, Louisiana Tech University, Ruston, LA, 71272, USA
[c] Department of Mechanical Engineering, University of Alabama, Tuscaloosa, UA, 35487, USA
[d] Departments of Aerospace Engineering and Mechanical Engineering, Iowa State University, Ames, IA, 50010, USA

ARTICLE INFO

Article history:
Received 25 March 2020
Received in revised form
30 April 2020
Accepted 14 May 2020
Available online 19 May 2020

ABSTRACT

Diamond is the hardest superhard material with excellent optoelectronic, thermomechanical, and electronic properties. Here, we have investigated the possibility of a new synthesis technique for diamane and diamond thin films from multilayer graphene at pressures far below the graphite → diamond transformation pressure. We have used the Molecular Dynamics technique with reactive force fields. Our results demonstrate a significant reduction (by a factor of two) in the multilayer graphene → diamond transformation stress upon using a combined shear and axial compression. The shear deformation in the multilayer graphene lowers the phase transformation energy barrier and plays the role of thermal fluctuations, which itself promotes the formation of diamond. We revealed a relatively weak temperature dependence of the transformation strain and stresses. The transformation stress vs. strain curve for the bulk graphite drops exponentially for finite temperatures.

1. Introduction

Diamond has unique properties such as ultra-hardness, reflectivity [1], high piezo-luminescence capacity [2], and high thermal conductivity [3]. Formation of atomically-thin diamond films from bi- and multi-layer graphene structures with unique thermophysical properties have recently been reported [4]. It has opened new doors to synthesize atomically-thin, low-dimensional devices for electromechanical and optoelectronic applications [5]. However, large-scale synthesis of these structures is hindered by the high pressures needed to initiate the graphene → diamond phase transformation [6,7]. Engineering the phase transformation kinetics can improve efficiency and reduce the costs for the synthesis of these materials. Different methods have been adopted, e.g., application of shear among the graphene layers [8], the saturation of the graphene layers by radical groups [4], and metallic catalyst [9,10].

Various theoretical and computational methods are utilized to study synthesis of 2D materials [11–15], specifically the diamondization process, e.g., Molecular Dynamics [7], DFT [4], and *ab initio*. [11,12] Among these methods, Molecular Dynamics has been widely used to study the phase transformation and surface effects in materials [17–24]. The solid-solid phase transformation, including the graphene → diamond transformation, is a complicated procedure. It depends on various parameters like defect quantity in the parent solid-phase, the direction of the compression with respect to the basal plane, local stress state, intermediate amorphous states, and surface energy [25–29].

A mechanism for the conversion of the hexagonal graphite to the diamond considering the martensitic nucleation under static compression has been proposed [30]. The formation of the cubic diamond was explained via a pole mechanism, i.e., the slip of transformation dislocations around the axial dislocation. A comparative study on the martensitic phase transformation of graphite-like structure, such as hexagonal boron nitride, has also been conducted under different loading schemes, i.e., static, hydrostatic, non-hydrostatic compression and shear-induced compression [31–35]. A pressure-induced phase transformation of multiwalled carbon nanotubes (MWCNT) to diamond has been reported [36], where stabilization of the formed diamond was investigated by applying shear stress via rotating one of the anvils. The activation of the phase transformation process in the unstable

* Corresponding author. Department of Mechanical Engineering, Louisiana Tech University, Ruston, LA, 71272, USA.
E-mail address: kmomeni@latech.edu (K. Momeni).

https://doi.org/10.1016/j.carbon.2020.05.038
0008-6223/

region, which results in the formation of a diamond phase, was demonstrated. Shear-driven phase transformation of glassy carbon to hexagonal diamond (HD) has recently been investigated [37], Fig. 1(a). Fig. 1(b) shows the formation of two regions of graphite and HD, which are separated by a region with a mixed composition of these two phases [37]. Shear driven synthesis of diamond using a rotating diamond anvil cell (RDAC) at subgigapascal pressure has been reported [16], Fig. 1(c–f). The formation of the cubic diamond (CD) was revealed, Fig. 1(c), while the presence of different structures (diamond and graphite) has been confirmed by Electron Energy Loss Spectrum (EELS), Fig. 1(d). The crystal planes and d-spacing of these planes are visible under high-resolution TEM (HRTEM) analysis in Fig. 1(e), and the presence of cubic diamond has been confirmed using the fast Fourier transformation (FFT), subfigure of Fig. 1(e). Formation of the orthorhombic diamond is visible along with the plane spacing under HRTEM, Fig. 1(f), and with selected area electron diffraction (SAED) and FFT analysis. The transformation stress of the cubic diamond formed under shearing DAC was reported to be lower than any other diamond phase.

Despite the recent success in lowering the graphite → diamond transformation pressure by applying shear during the experimental synthesis process, a fundamental understanding of the mechanisms governing this lower pressure transformation is still missing. Here, we have used Molecular Dynamics method with the Long-range Carbon Bond Order Potential (LCBOP) reactive force field to understand the atomistic mechanisms governing the phase transformation. We have investigated the effect of loading dynamics, thickness, and the surface on the kinetics of diamondization from multilayer graphene and graphite structures. We also considered the diamondization under axial compression for comparison. Our results demonstrate that introducing shear during the compression can reduce the critical phase transformation strain by up to 40%.

2. Computational model

The bulk graphite and different multilayer graphene structures are studied. The initial interlayer distance between graphene layers is assumed to be the length of the π-bond between carbon atoms in adjacent graphene layers, i.e., 3.4 Å [38]. We placed one graphene layer on top of the other layer while shifting the second layer by 1.41 Å, i.e., length of the C–C bond, to form the ABAB stacking where carbon atoms in one layer are in the middle of the hexagonal carbon ring of the adjacent layer. The structure, crystallography directions, and coordinate axis are shown in Fig. 2. The crystallography axis are $\boldsymbol{a}_1 = a(\sqrt{3}/2, -1/2, 0)$, $\boldsymbol{a}_2 = a(\sqrt{3}/2, 1/2, 0)$, $\boldsymbol{a}_3 = c(0, 01)$, where $|\boldsymbol{a}_1| = |\boldsymbol{a}_2| = a = 2.46$Å, and $|\boldsymbol{a}_3| = c = 6.71$Å. The coordinate axis are $\boldsymbol{x} = (\boldsymbol{a}_1 + \boldsymbol{a}_2)/|\boldsymbol{a}_1 + \boldsymbol{a}_2|$, $\boldsymbol{y} = (\boldsymbol{a}_2 - \boldsymbol{a}_1)/|\boldsymbol{a}_2 - \boldsymbol{a}_1|$, and $\boldsymbol{z} = \boldsymbol{a}_3$.

Interatomic Interactions Model — Different interatomic potentials, e.g., AIREBO [39], LCBOP [40], and ReaxFF [41], are developed to reproduce the mechanical properties of all forms of carbon allotropes [42–44] that match the experimentally reported values. Among the aforementioned interatomic potentials, only the LCBOP [40] potentials could pass our test cases. The other two potentials incurred unphysical instability problems during our first test simulations. Thus, we performed our studies using the LCBOP [40]

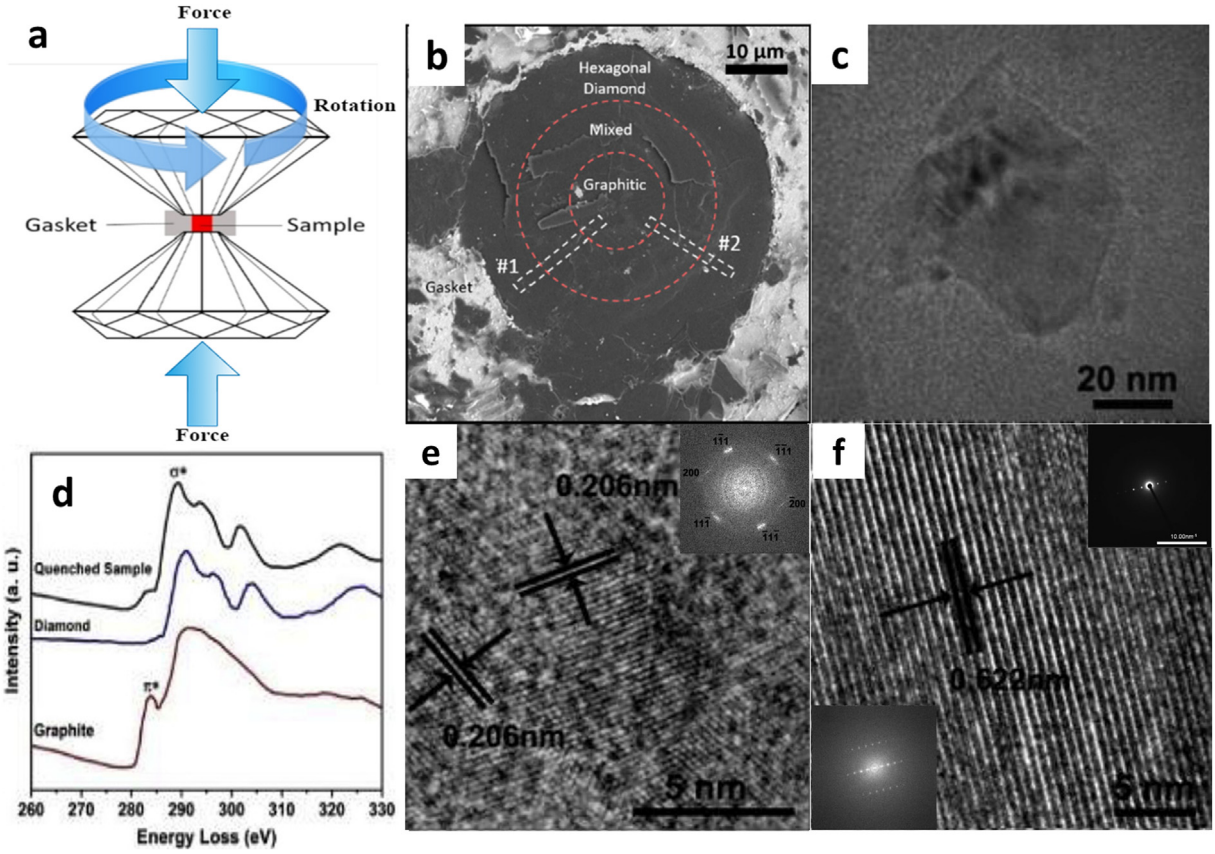

Fig. 1. Formation of diamond under combined compression and shear. **(a)** Schematic of the experimental setup; **(b)** SEM image of the mixed graphite and HD phases after compression in the DAC; **(c)** TEM image of a nanocrystalline CD; **(d)** intensity spectrum comparison of graphite and formed diamond; **(e)** HRTEM image of the cubic diamond nanocrystal and FFT analysis showing crystal planes; **(f)** HRTEM of an orthorhombic diamond along with the FFT (upper right) and SAED (lower left) analysis. (a–b) Reprinted from Ref. [37] with permission from Elsevier; and (c–f) Reprinted from Ref. [16] with permission from Elsevier. (A colour version of this figure can be viewed online.)

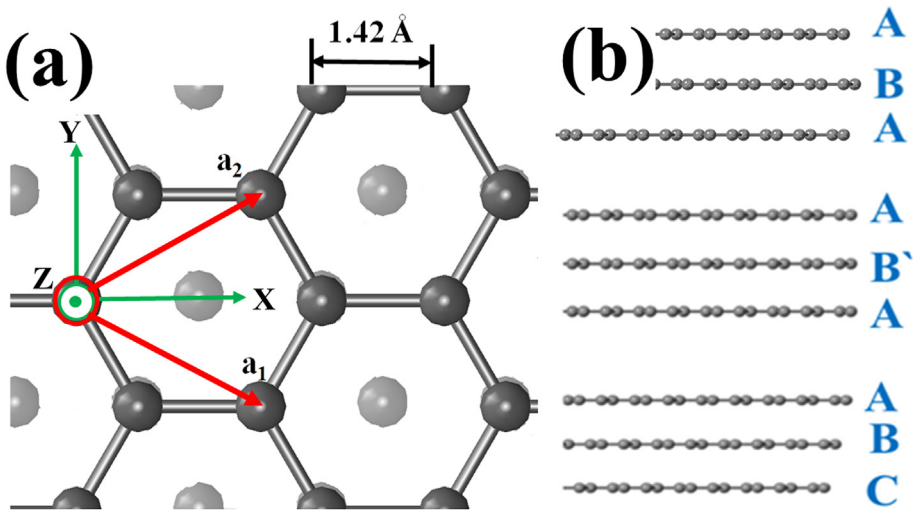

Fig. 2. Structure and configuration of the modeled system. (a) Top view of the multilayer graphene structure with ABAB stacking along with the crystallography (a_1, a_2, a_3) and coordinate system (x,y,z) directions. (b) Different stackings of multilayer graphene structures, where the ABA stacking is considered for our studies. (A colour version of this figure can be viewed online.)

potential. LCBOP is considered as a powerful potential for carbon, which captures chemical and physical phenomena not only in the bonded interaction like covalent bond with various hybridizations but also the long-range non bonded interactions such as those between graphene layers. Also, this potential has successfully been used to study high-pressure phases of carbon [45]. The slipping and shearing phenomenon of graphene layers have been successfully described by this LCBOP [46] and its derivative potentials [45]. This potential can capture the nonbonded interactions between the graphite layers, as well as a hybridized covalent bond. These capabilities qualify this potential to implement in our study.

The binding energy E between two carbon atoms for the LCBOP potential is defined as

$$E_b = \frac{1}{2}\sum_{i,j}^{N} V_{ij}^{tot} = \frac{1}{2}\sum_{i,j}^{N}\left(f_{c,ij}V_{ij}^{SR} + S_{ij}V_{ij}^{LR}\right), \tag{1}$$

where V_{ij}^{tot} is the total interatomic interaction which is the sum of short-range V_{ij}^{SR} and the long-range V_{ij}^{SR} interactions. The $f_{c,ij}$ is a smooth cutoff function and S_{ij} is a switching function. V_{ij}^{SR} is the function of attractive and repulsive pair potentials and contains the bond order B_{ij} parameter

$$V_{ij}^{SR} = V_R(r_{ij}) - B_{ij}V_A(r_{ij}). \tag{2}$$

The attraction and the repulsion interaction term have been obtained by fitting binding energies, lattice constants, and isotropic elastic properties for various polytypes of carbon.

$$V_R(r) = Ae^{-\alpha r}; \tag{3}$$

$$V_A(r) = B_1 e^{-\beta_1 r} + B_2 e^{-\beta_2 r}. \tag{4}$$

The B_{ij} parameter dependents on the bond angle and conjugation effect in the bond interaction.

$$B_{ij} = \frac{1}{2}\left[b_{ij} + b_{ji} + F^{conj}\left(N_{ji},\ N_{ji}, N_{ij}^{conj}\right)\right], \tag{5}$$

where b_{ji} is the angular dependent term and F^{conj} is the conjugation part of the bond order. The LCBOP potential includes the dihedral terms along with van der Waals's long-range interaction, which will correctly maintain the stacking sequences of graphene layers even during graphene shearing and the phase change from graphene to diamond. Moreover, it captures the sp^2 to sp^3 hybridization phenomena, therefore, bond breaking and formation that's involved with the graphene to diamond phase transformation.

Using the LCBOP potential, we studied diamondization of multilayer graphene and bulk graphite systems under axial compression and combined axial/shear loading. Details of setting up the associated simulations are elaborated below. We considered an ABAB stacking sequence of graphene layers, Fig. 2(b).

In our study, we have taken the transformation stress data when at least 10% graphene/graphitic structure has transformed into a diamond. The Cauchy stresses reported in this study were calculated by the virial stress theorem as follows [47,48].

$$\sigma_{ij} = \frac{1}{\Omega^{\alpha}}\left(\frac{1}{2}m^{\alpha}v_i^{\alpha}v_j^{\alpha} + \sum_{\beta=1,n}^{n} r_{\alpha\beta}^{j}f_{\alpha\beta}^{i}\right). \tag{6}$$

Here i and j denote indices in the Cartesian coordinate system; α and β are the atomic indices; m^{α} and v^{β} denote the mass and velocity of atom α; $r_{\alpha\beta}$ is the distance between atoms α and β, and Ω is the atomic volume of atom α. For virial stress calculations, we have used the total atomic volume of the system. For strain calculation, we have used the summation of atomic strains. The compressive and transformation stress and strain tensors are designated with subscript c and superscript t, respectively. Here we have used the per atomic stress for calculating transformation stress, and we have used VMD [10] to get the exact atomic strain for all the simulations.

Multilayer graphene – A simulation cell of 56.54 × 26.41 Å in the plane of graphene layers is considered to model multilayer graphene structures. We applied a non-periodic and moving, i.e., shrink-wrapped, boundary condition in the direction normal to the graphene's plane with empty spaces of 10A in thickness on top and bottom surfaces. We considered two loading scenarios for comparison: (i) axial compression, and (ii) combined compression and shear. For the case of axial compression, an interactive wall potential could be applied. However, because of the limitation of the interactive wall for applying shear loads, we did not use it for investigating either axial compression or the shearing process. Instead, we added two extra layers of graphene on each of the top and bottom sides and applied compression by moving the top

graphene layer downward while keeping the bottom layer fixed. The combined loading was performed through a sequence of compression and shearing, where shearing of the sandwiched graphene layers is achieved by moving the top graphene layer in its plane. All the analysis and calculated properties are for the graphene layers sandwiched between the two top and bottom graphene layers.

For axial compression loading, we relaxed the structure for 80ps after every step of compression. The compression step was 0.3A for initial steps and reduced to 0.01A, when strain in the z-direction (see Fig. 2) reaches 16% to avoid the unwanted atomic collision between the layers. For the combined compression with shear loading, the structure has been relaxed for 8ps after each compression, and then we displaced the top layer by 2.45A, i.e., the furthest C–C distance, in 10 steps. After each shearing step, the structure was relaxed for 10ps. The stability of the formed diamond was investigated by removing the compressive stress while monitoring any phase transformations. This was achieved by moving the top graphene layer up to its original position. All the loading and unloading processes are performed under the NVT ensemble.

Bulk graphite – We further studied phase transformation for the bulk graphite to understand the surface effects on the nucleation and growth of diamond. A graphite structure with nine layers (9L) of graphene is considered with simulation cell dimensions of 14.12 × 12.76 × 30.60 Å with periodic boundary conditions in all directions. We compress the structure by deforming the simulation box in the z-direction at a strain rate of 1A/fs. For shearing the bulk graphene structure, we took different compressed structures and sheared them at a rate of 0.02 Å/ps in the x-direction (Fig. 2) for 300ps. We performed all the loadings under the NPT ensemble.

3. Result analysis and discussion

The energy of bulk graphite as a function of shear strain for different compressive stresses at zero and a finite temperature (600K) is plotted in Fig. 3. The results show the formation of the first diamond structure at ~15% shear strain and 26.4% compressive Lagrangian strain. This condition corresponds to the first drop in the energy curve. The formed diamond structure vanished upon applying further shear, which accompanies an increase in the energy of the system. When the graphene layers come in a proper stacking orientation with the help of applied shear, then diamond forms, and as the shear goes further, the structure loses its favorable stacking condition for diamond formation. Comparing Fig. 3(a) and (b) reveals that the phase transformation energy is temperature-dependent. The energy landscape for 1200K is also given in the Supplementary Information, which indicates the increase in the transformation energy by increasing temperature.

We have included the energy vs. strain plot for at 0K and 600 to emphasize the variation of the shear strain and energy relation with the temperature. The phase transformation occurs at a larger compressive strain at elevated temperatures. The increase in the transformation energy, which indicates the increase in the phase transformation energy barrier [27], as well as an increase in the transformation strain, could be interpreted by the thermal strains. A larger compressive strain is needed to overcome the excess thermal expansion strains in addition to the phase transformation strain. Fig. 3(a) indicates that the phase transformation energy, which is equivalent to the drops on the energy curve, remains relatively constant by increasing the compressive strain, although the total energy of the sample increases.

The energy vs. shear plot at 0K, Fig. 3, reveals a sawtooth shape, which transforms into a smooth curve at 600K. At higher temperatures, the degree of disordering increases, which is a prime factor for increasing its lubricity [49]. The viscosity or lubricity of the graphene-like structure is one of the dominating factors for their smooth shearing, which explains the smooth energy transition at 600K. Fig. 3(a) shows an even distribution trend, as the diamond fraction is almost constant after transformation under different shear loadings, Fig. 3(c). The diamond fractions have been identified and calculated by the OVITO [50] visualization software. The energy vs. shear plot for a finite temperature shows ascending or descending trends depending on the transformation energy released during each graphene → diamond phase transformation, Fig. 3(b). During the simulation of the lowest compressed structure (29.00% strain), the diamond percentage becomes very low in the final steps of shearing simulation, Fig. 3(d). Therefore, the energy required to shear graphene layers decreases as there are not many interlayer covalent bonds to break. For shearing of the graphene layers, only the van der Waals attraction needs to be overcome for this structure compressed with a 29% strain.

In Fig. 3(a) for 0K temperature, simulations are performed for compressive strains which are very close to each other because the structure compressed less than 26.4% strain did not form any diamond upon the shearing and the structure compressed with a higher strain beyond 26.50% had been partially transformed to the diamond without applying shear. For the 600K, we have chosen these particular compressive strains so that we can show the energy variation during the shearing of the phase transformation. Beyond the 30%, the structure transformed to diamond, and beneath 29% compressive strain, we have not seen any diamond formation even after applying the shear.

We further studied the graphene → diamond phase transformation in the bulk graphite, Fig. 4, to understand the effect of surfaces on the thermodynamics and kinetics of this phase transformation. Our results on axial compression simulations of the bulk graphite show that 90% of the graphite structure transformed to the diamond at 35% compressive strain, which is observed as a jump in the stress-strain curve Fig. 4(a). To study the effect of shearing on the phase transformation kinetics, we compressed the bulk graphite structure at various temperatures and used the compressed structures at different stages before the nucleation of the diamond as the *initial structure for shearing simulations*. Here, the transformation stress is defined as the stress required to transform at least 10% of the sample to diamond. Results presented in Fig. 4 (b) revealed that increasing the shear stress will exponentially reduce the transformation stress until it reaches a constant value. The applied shear load reorients the covalent bonds and thus makes them weaker, resulting in a phase transformation. The atoms at 0K have specific positions due to lacking any thermal vibrations. As a result, nucleation is barrierless at the lattice instability conditions. The diamond structure showed up when the convenient atomic orientation comes due to the continuous shear and vanishes all of a sudden when the atomic orientation gets missing. Therefore, we have seen a sudden drop in the energy curve of the 0K in Fig. 3(a).

On the other hand, at nonzero temperatures, thermal fluctuations cause thermally-activated nucleation before lattice instability is reached. Breaking and formation of symmetry are based on the average position of atoms, and that is why we have seen a gradual change in the diamond fraction during the simulation of non-zero temperature rather than jump-like complete phase transformation. Therefore, we observed continuous energy changes for 600K in Fig. 3(b). For the 0K, red hexagonal dots in Fig. 4(b), the effect of shear stress in the reduction of transformation stress is negligible. Furthermore, the transformation stress increases by increasing temperature up to 600K, where it drops and then starts to increase again as temperature increases. This complex response can be interpreted using the competition between the increase in thermal expansion and a reduction in the energy barrier for the phase transformation. For the initial increase in temperature, thermal

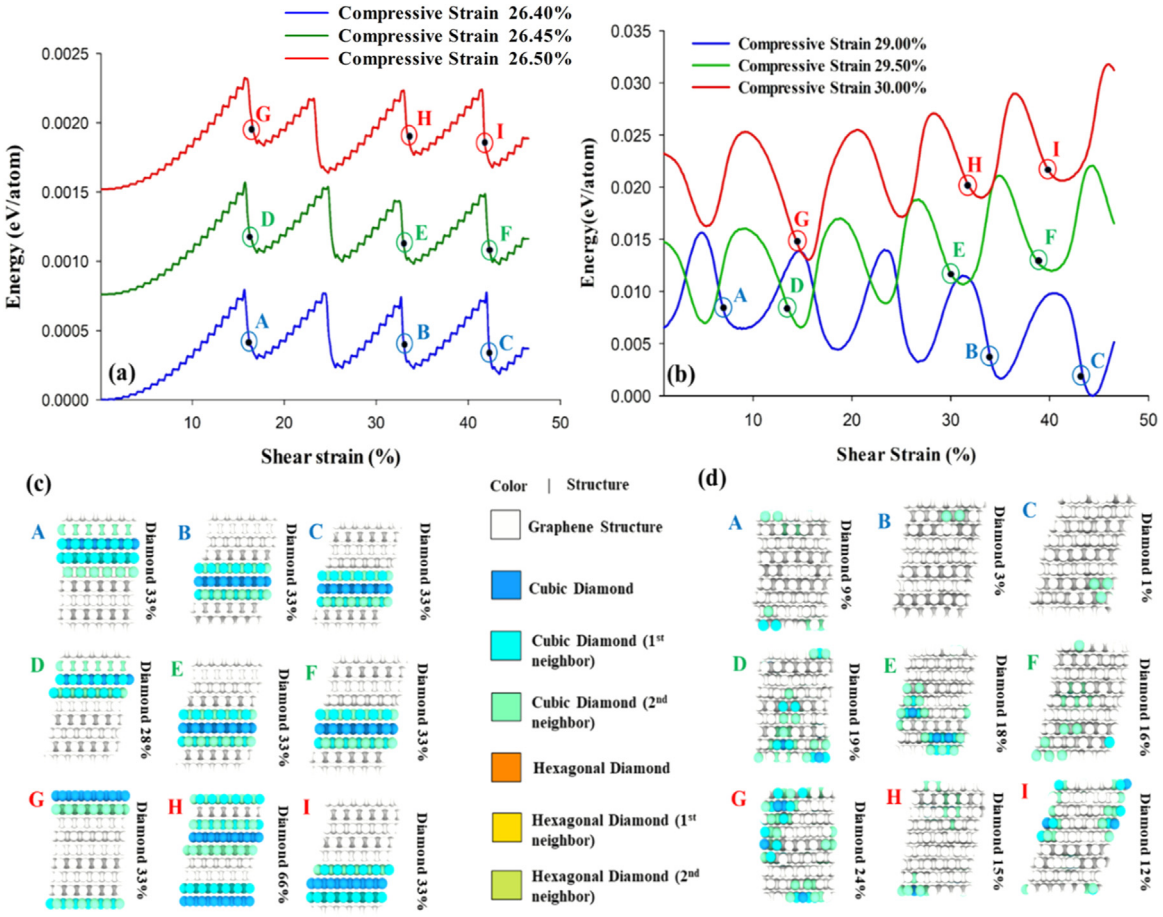

Fig. 3. Energy of graphite as a function of shear strain at different compressive strains for an 8L graphene system at 0K (a) and 600K (b); The energy values are normalized (shifted with respect to the minimum global energy) over per-atom energy value. (c), and (d) represent the structure corresponding to the selected points in the plot (a) and (b). (A colour version of this figure can be viewed online.)

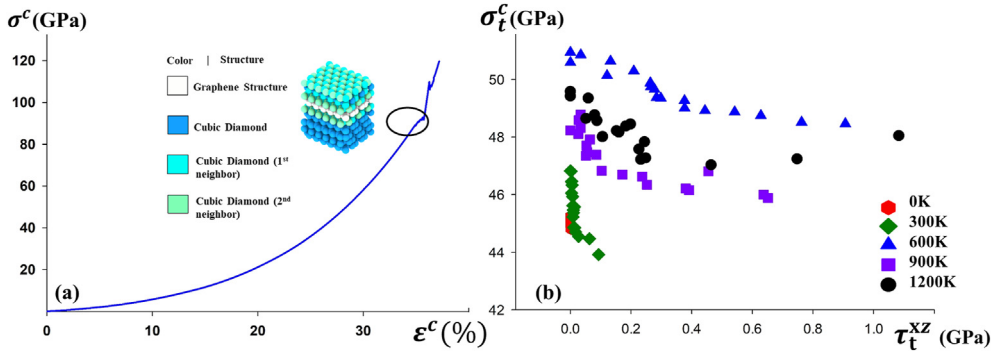

Fig. 4. Bulk graphite simulation results. (a) Stress-strain curve for axial compression loading. Transformation strain is detectible as a jump in the stress-strain curve, at ~35% for 0K temperature. (b) Transformation stress vs. shear stress for bulk graphite for various temperatures. Transformation stress is defined as the stress required to transform at least 10% of the sample to diamond. Transformation stress reaches a plateau by increasing shear stress. It also increases by increasing temperature, while it has a maximum at 600K. (A colour version of this figure can be viewed online.)

expansion of the structure results in the need for an increase in the critical pressure for initiation of the phase transformation, i.e., transformation stress. However, in an opposite effect, higher temperature increases the contribution from thermal fluctuations and reduces the pressure required for initiating the phase transformation. The reduction in phase transformation due to the contribution of thermal fluctuations will be dominant at elevated temperatures.

We further investigated the phase transformation stress and strain as functions of temperature and number of graphene layers, Fig. 5. Here, we have considered phase transformation stresses and strains as the ones at which 10% of the sample transformed into a diamond. Our results indicate a direct correlation between the transformation stress and temperature. The exceptions to this rule are the 3L and 5L structures at 0K, where the added thermal fluctuations were enough to overcome the phase transformation

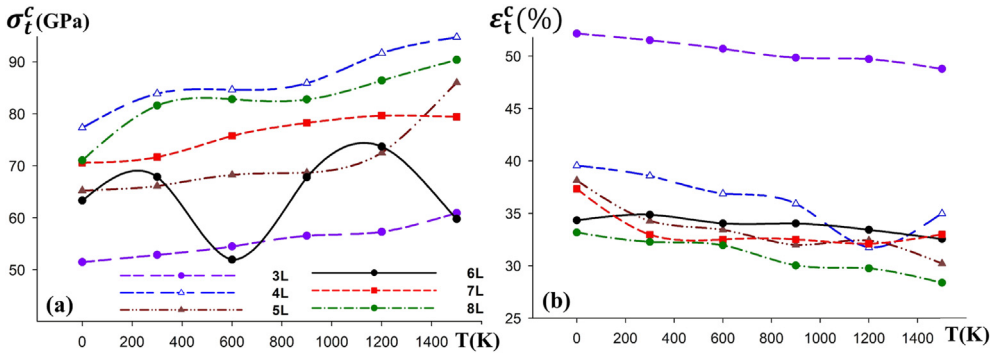

Fig. 5. Variation of the transformation stress and strain as a function of temperature under axial compression for multilayer graphene systems. (a) Transformation stress and (b) transformation strain for the graphene → diamond phase transformation. The phase transformation is defined as the stress and strain at which 10% of the sample transforms to diamond during axial compression. While the transformation stress is directly correlated with temperature, transformation strain is only a weak function of temperature. (A colour version of this figure can be viewed online.)

barrier, while the additional thermal strain was minor. The compressive transformation stress for the 6L structure fluctuates with temperature variations at 600K and 1500K, where the diamond concentration can explain it. In the case of 600K and 1500K, the diamond percentage jumps up to 75% and 90%, respectively, right after the transformation.

On the contrary, for other temperatures, the phase transformation to diamond seems more gradual, and diamond fraction goes to 20–30% initially after transformation. Therefore, we have seen a sudden drop in the transformation stress in the case of 600K and 1500K temperatures. The transformation stress is also a strong function of the number of the graphene layers, and increases with the number of the layers, except for the 4L structure, which has the highest transformation stresses in the modeled multilayer graphene systems. The volume fraction of diamond in the 4L structure does not increase gradually and instead jumps to 70–80%, which explains its very high transformation stress. Our results, Fig. 5(b), indicate that the transformation strain is a weak function of temperature, which is consistent with the experimental measurements [51]. The transformation strain increases with the layer number, except for the 3L structure, which has the largest transformation strain due to the dominant surface effects.

Variation of transformation stress and strain as functions of temperature are shown in Fig. 6 for multilayer graphene structures for combined compression and shear loading. Here, the structure was compressed in the z-direction incrementally, where after each compression step, the structure was sheared in the x-direction for one unit cell. The reported transformation stresses and strains correspond to the values of stress and strain, were at least 10% of the model material transformed to diamond. Our results indicate that the transformation stress reduces by a factor of two compared to the axial compression, Fig. 5(a). Thus, shear in the plane of graphene layers facilitates slipping of the graphene layers to a configuration that helps the formation of the interlayer C–C bonds at lower compressive stress.

Furthermore, the transformation stress has a direct correlation with the temperature. The variation of transformation strain as a function of temperature for the combined shear and compression loading is shown in Fig. 6(b). These results indicate that the transformation strain under combined loading decreases by ~10% over the temperature of 1400K, and it increases with the number of layers for systems with an odd number of graphene layers. For the systems with an even number of layers, we could not detect a clear pattern, which could be explained by the fact that a single diamond unit cell requires at least three graphene layers to form. Thus, the formation of an integer number of diamond unit cells is not feasible for systems with an even number of graphene layers, which hinders the gradual formation of the diamond and detection of a pattern. This condition cannot easily be required to form the fact that a diamond unit cell. Comparing the reduction of the transformation stress under shear loading in the bulk graphite (Fig. 4(b)) and multilayer graphene (Fig. 6(b)) reveals that this reduction is more significant for the multilayer graphene system. Thus, the surface effects have a significant role in the graphene → diamond phase transformation.

Experimental investigations reported a reduction in the

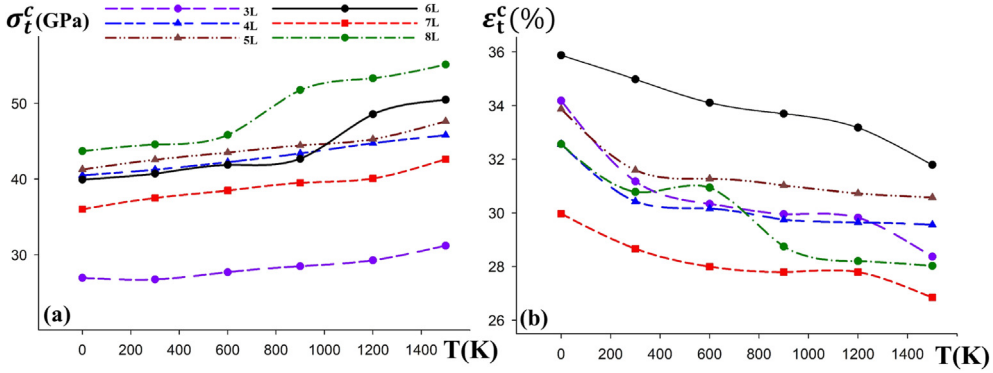

Fig. 6. Transformation stress and strain as a function of temperature under combined compression and shear loading. Transformation stress (a) and transformation strain (b) for the graphene → diamond phase transformation under the combined compression and shear. The structure was compressed and sheared at the same time. The reported values are the transformation stress/strain at a minimum shear, which results in the formation of at least 10% diamond. The results indicate a reduction in the transformation stress by a factor of two when shear applies. (A colour version of this figure can be viewed online.)

transformation stress to 0.7 GPa at 300K [16], which is smaller than what we revealed using the Molecular Dynamics simulations. This difference could be due to differences in the number of layers, surface conditions such as lack of atomically flat surfaces on the diamond anvils, and ambiguity in the critical volume fraction of diamond used to determine the transformation pressure. Furthermore, in our simulations, we only consider diamond formation if the atoms satisfy the exact symmetry and bond distances of a diamond phase. This assumption is in contrast to experimental measurements that report the formation of diamond based on the aggregated symmetry of a transformed volume and are less sensitive to the bond distance. Also, preventing any contamination from presenting in the experiments is not practically viable, which can further reduce the barrier for the transformation of graphite to diamond. A similar issue of having a higher phase transformation stress in simulations compared to the experiments have also been reported for the bulk graphite → diamond phase transformation [16,52]. Particularly DFT simulations have also reported a reduction in the transformation stress when shear forces are applied, which is consistent with presented results [16]. Getting the full picture of the reason behind this discrepancy requires further investigation and close collaboration between theoreticians and experimentalists.

4. Conclusion

We have investigated the effect of the superposed shear stress on the thermodynamics and kinetics for the transformation of graphite and multilayer graphene to diamond, using the Molecular Dynamics technique with reactive force fields. Specifically, the effects of loading type (axial compression or compression with shear), temperature, and thickness of the multilayer graphene structure are studied. Defining the phase transformation stress and strain as the values in which at least 10% of the material transforms to diamond, we revealed that the transformation stress normal to the plane of graphene layers can be reduced by a factor of two by superposing a shear force for bulk graphite and multi-layered graphene structures. We revealed that the transformation stress normal to the graphene planes, σ_t^c, reduces by increasing the applied shear stress, and shows a weak dependence on temperature. The transformation strain is also a weak function of temperature, which is consistent with previous reports [7].

We discovered that transition from a jump-like phase transformation of bulk graphite to the diamond at 0K, to a continuous phase transition at finite temperatures, which was associated with the transition from barrierless to thermally-activated nucleation. This study of shear driven phase transformation from multilayer graphene and graphite structures to diamond can guide the synthesis of stable diamine and thin diamond films at industrial scales with implications in electronics, defense, and coating industries.

Declaration of competing interest

The authors declare that they have no known competing financial interests or personal relationships that could have appeared to influence the work reported in this paper.

CRediT authorship contribution statement

Shiddartha Paul: Software, Validation, Formal analysis, Investigation, Writing - original draft, Visualization. **Kasra Momeni:** Conceptualization, Methodology, Validation, Formal analysis, Resources, Data curation, Writing - original draft, Supervision, Project administration, Funding acquisition. **Valery I. Levitas:** Formal analysis, Writing - review & editing.

Acknowledgment

This project is also partly supported by DoE-ARPA-E OPEN, NASA-EPSCoR, Louisiana EPSCoR-OIA-1541079 (NSF(2018)-CIMM-Seed-18 and NSF(2018)-CIMMSeed-19), LEQSF(2015-18)-LaSPACE, Louisiana Tech University, the National Science Foundation 2D Crystal Consortium – Material Innovation Platform (2DCC-MIP) under NSF cooperative agreement DMR-1539916, and the NSF-CAREER under NSF cooperative agreement CBET-1943857. VIL was supported by NSF (CMMI-1943710 and MMN-1904830), ARO (W911NF-17-1-0225), and ONR (N00014-16-1-2079).

Appendix A. Supplementary data

Supplementary data to this article can be found online at https://doi.org/10.1016/j.carbon.2020.05.038.

References

[1] A.M. Bonnot, B.S. Mathis, S. Moulin, Investigation of the growth kinetics of low pressure diamond films by in situ elastic scattering of light and reflectivity, Appl. Phys. Lett. 63 (1993) 1754–1756, https://doi.org/10.1063/1.110704.
[2] G. Davies, Dynamic Jahn-Teller distortions at trigonal optical centres in diamond, J. Phys. C Solid State Phys. 12 (1979) 2551–2566, https://doi.org/10.1088/0022-3719/12/13/019.
[3] J. Che, T. Çağın, W. Deng, W.A. Goddard, Thermal conductivity of diamond and related materials from molecular dynamics simulations, J. Chem. Phys. 113 (2000) 6888–6900, https://doi.org/10.1063/1.1310223.
[4] Y. Gao, T. Cao, F. Cellini, C. Berger, W.A. De Heer, E. Tosatti, E. Riedo, A. Bongiorno, Ultrahard Carbon Film from Epitaxial Two-Layer Graphene, vol. 13, 2018.
[5] Light-Induced Plasmon-Assisted Phase Transformation of Carbon on Metal Nanoparticles - Kulkarni - 2012 - Advanced Functional Materials - Wiley Online Library, (n.d.).
[6] H. Sumiya, H. Yusa, T. Inoue, H. Ofuji, T. Irifune, Conditions and mechanism of formation of nano-polycrystalline diamonds on direct transformation from graphite and non-graphitic carbon at high pressure and temperature, High Press Res. 26 (2006) 63–69, https://doi.org/10.1080/08957950600765863.
[7] S. Paul, K. Momeni, Mechanochemistry of stable diamane and atomically thin diamond films synthesis from Bi- and multilayer graphene: a computational study, J. Phys. Chem. C 123 (2019) 15751–15760, https://doi.org/10.1021/acs.jpcc.9b02149.
[8] Y. Peng, L. Xiong, CRYSTAL orientation dependence OF mechanical and thermal properties IN atomistic computational analysis of the loading orientation-dependent phase transformation in graphite under compression, JOM (2019) 19–23, https://doi.org/10.1007/s11837-019-03726-y.
[9] M. Akaishi, H. Kanda, S. Yamaoka, High pressure synthesis of diamond in the systems of grahpite-sulfate and graphite-hydroxide, Jpn. J. Appl. Phys. 29 (1990) L1172–L1174, https://doi.org/10.1143/JJAP.29.L1172.
[10] M. Akaishi, H. Kanda, S. Yamaoka, Synthesis of diamond from graphite-carbonate system under very high temperature and pressure, J. Cryst. Growth 104 (1990) 578–581, https://doi.org/10.1016/0022-0248(90)90159-I.
[11] N. Briggs, S. Subramanian, Z. Lin, X. Li, X. Zhang, K. Zhang, K. Xiao, D. Geohegan, R. Wallace, L.Q. Chen, M. Terrones, A. Ebrahimi, S. Das, J. Redwing, C. Hinkle, K. Momeni, A. Van Duin, V. Crespi, S. Kar, J.A. Robinson, A roadmap for electronic grade 2D materials, 2D Mater. (2019), https://doi.org/10.1088/2053-1583/aaf836.
[12] F. Zhang, K. Momeni, M.A. AlSaud, A. Azizi, M.F. Hainey, J.M. Redwing, L.Q. Chen, N. Alem, Controlled synthesis of 2D transition metal dichalcogenides: from vertical to planar MoS2, 2D Mater. (2017), https://doi.org/10.1088/2053-1583/aa5b01.
[13] R.A. Vilá, K. Momeni, Q. Wang, B.M. Bersch, N. Lu, M.J. Kim, L.Q. Chen, J.A. Robinson, Bottom-up synthesis of vertically oriented two-dimensional materials, 2D Mater. 3 (2016), 041003, https://doi.org/10.1088/2053-1583/3/4/041003.
[14] K. Momeni, Y. Ji, K. Zhang, J.A. Robinson, L.-Q. Chen, Multiscale framework for simulation-guided growth of 2D materials, Npj 2D Mater. Appl. 2 (2018) 27, https://doi.org/10.1038/s41699-018-0072-4.
[15] R.Z. Khaliullin, H. Eshet, T.D. Kühne, J. Behler, M. Parrinello, Nucleation mechanism for the direct graphite-to-diamond phase transition, Nat. Mater. 10 (2011) 693–697, https://doi.org/10.1038/nmat3078.
[16] Y. Gao, Y. Ma, Q. An, V. Levitas, Y. Zhang, B. Feng, J. Chaudhuri, W.A. Goddard III, Shear driven formation of nano-diamonds at sub-gigapascals and 300 K, Carbon 146 (2019) 364–368.
[17] K. Momeni, Y. Ji, Y. Wang, S. Paul, S. Neshani, D.E. Yilmaz, Y.K. Shin, D. Zhang, J.-W. Jiang, H.S. Park, others, Multiscale computational understanding and growth of 2D materials: a review, Npj Comput. Mater. 6 (2020) 1–18.
[18] H. Attariani, S.E. Rezaei, K. Momeni, Mechanical property enhancement of one-dimensional nanostructures through defect-mediated strain engineering,

Extrem. Mech. Lett. 27 (2019) 66–75, https://doi.org/10.1016/j.eml.2019.01.004.
[19] H. Attariani, K. Momeni, K. Adkins, Defect engineering: a path toward exceeding perfection, ACS Omega 2 (2017) 663–669. http://pubs.acs.org/doi/abs/10.1021/acsomega.6b00500.
[20] H. Attariani, S. Emad Rezaei, K. Momeni, Defect engineering, a path to make ultra-high strength low-dimensional nanostructures, Comput. Mater. Sci. 151 (2018), https://doi.org/10.1016/j.commatsci.2018.05.005.
[21] M. Ghosh, S. Ghosh, H. Attariani, K. Momeni, M. Seibt, G. Mohan Rao, Atomic defects influenced mechanics of II-VI nanocrystals, Nano Lett. 16 (2016), https://doi.org/10.1021/acs.nanolett.6b00571.
[22] K. Momeni, G.M. Odegard, R.S. Yassar, Finite size effect on the piezoelectric properties of ZnO nanobelts: a molecular dynamics approach, Acta Mater. 60 (2012), https://doi.org/10.1016/j.actamat.2012.06.041.
[23] K. Momeni, H. Attariani, Electromechanical properties of 1D ZnO nanostructures: nanopiezotronics building blocks, surface and size-scale effects, Phys. Chem. Chem. Phys. 16 (2014), https://doi.org/10.1039/c3cp54456g.
[24] K. Momeni, H. Attariani, R.A. Lesar, Structural transformation in monolayer materials: a 2D to 1D transformation, Phys. Chem. Chem. Phys. 18 (2016) 19873–19879, https://doi.org/10.1039/c6cp04007a.
[25] Y. Peng, F. Wang, Z. Wang, A.M. Alsayed, Z. Zhang, A.G. Yodh, Y. Han, Phase Transitions, 2014, https://doi.org/10.1038/NMAT4083.
[26] K. Momeni, V.I. Levitas, Propagating phase interface with intermediate interfacial phase: phase field approach, Phys. Rev. B 89 (2014) 184102, https://doi.org/10.1103/PhysRevB.89.184102.
[27] V.I. Levitas, K. Momeni, Solid–solid transformations via nanoscale intermediate interfacial phase: multiple structures, scale and mechanics effects, Acta Mater. 65 (2014) 125–132.
[28] K. Momeni, V.I. Levitas, J.A. Warren, The strong influence of internal stresses on the nucleation of a nanosized, deeply undercooled melt at a solid–solid phase interface, Nano Lett. 15 (2015) 2298–2303.
[29] K. Momeni, V.I. Levitas, A phase-field approach to nonequilibrium phase transformations in elastic solids via an intermediate phase (melt) allowing for interface stresses, Phys. Chem. Chem. Phys. 18 (2016) 12183–12203, https://doi.org/10.1039/C6CP00943C.
[30] V.F. Britun, A.V. Kurdyumov, I.A. Petrusha, dep20@ipms.kiev.ua, diffusionless nucleation of lonsdaleite and diamond in hexagonal graphite under static compression, Powder Metall. Met. Ceram. 43 (2004) 87–93, https://doi.org/10.1023/B:PMMC.0000028276.63784.8e.
[31] V.F. Britun, A.V. Kurdyumov, Analysis of influence of non-hydrostatic conditions of compression on phase transformations in carbon, Poroshkovaya Metall. 41 (2002) 92–99.
[32] V.F. Britun, A.V. Kurdyumov, Mechanisms of martensitic transformations in boron nitride and conditions of their development, High Pres. Res. 17 (2000) 101–111, https://doi.org/10.1080/08957950008200933.
[33] V.I. Levitas, Y. Ma, J. Hashemi, M. Holtz, N. Guven, Strain-induced disorder, phase transformations, and transformation-induced plasticity in hexagonal boron nitride under compression and shear in a rotational diamond anvil cell: in situ x-ray diffraction study and modeling, J. Chem. Phys. 125 (2006) 44507.
[34] C. Ji, V.I. Levitas, H. Zhu, J. Chaudhuri, A. Marathe, Y. Ma, Shear-induced phase transition of nanocrystalline hexagonal boron nitride to wurtzitic structure at room temperature and lower pressure, Proc. Natl. Acad. Sci. U.S.A. 109 (2012) 19108–19112, https://doi.org/10.1073/pnas.1214976109.
[35] V.I. Levitas, L.K. Shvedov, Low-pressure phase transformation from rhombohedral to cubic BN: experiment and theory, Phys. Rev. B 65 (2002) 104109.
[36] V. Blank, V. Churkin, B. Kulnitskiy, I. Perezhogin, A. Kirichenko, S. Erohin, P. Sorokin, M. Popov, Pressure-induced transformation of graphite and diamond to onions, Crystals 8 (2018) 68, https://doi.org/10.3390/cryst8020068.
[37] S. Wong, T.B. Shiell, B.A. Cook, J.E. Bradby, D.R. Mckenzie, D.G. Mcculloch, The shear-driven transformation mechanism from glassy carbon to hexagonal diamond, Carbon 142 (2019) 475–481, https://doi.org/10.1016/j.carbon.2018.10.080.
[38] S. Plimpton, Range Molecular Dynamics 1 Introduction, for Short { 117, 1995, pp. 1–42.
[39] S.J. Stuart, A.B. Tutein, J.A. Harrison, A reactive potential for hydrocarbons with intermolecular interactions A simple nonequilibrium molecular dynamics method for calculating the thermal conductivity A reactive potential for hydrocarbons with intermolecular interactions, J. Chem. Phys. 112 (2000) 24903–24926, https://doi.org/10.1063/1.3488620.
[40] H. Los, A. Fasolino, Intrinsic long-range bond-order potential for carbon: performance in Monte Carlo simulations of graphitization, Phys. Rev. B Condens. Matter 68 (2003) 1–14, https://doi.org/10.1103/PhysRevB.68.024107.
[41] A.C.T. Van Duin, S. Dasgupta, F. Lorant, W.A. Goddard, ReaxFF: a reactive force field for hydrocarbons, J. Phys. Chem. 105 (2001) 9396–9409, https://doi.org/10.1021/jp004368u.
[42] J.A. Baimova, L.K. Rysaeva, A.I. Rudskoy, Deformation behavior of diamond-like phases: molecular dynamics simulation, Diam. Relat. Mater. 81 (2018) 154–160.
[43] J.A. Baimova, B. Liu, S. V Dmitriev, N. Srikanth, K. Zhou, Mechanical properties of bulk carbon nanostructures: effect of loading and temperature, Phys. Chem. Chem. Phys. 16 (2014) 19505–19513.
[44] H. Zhan, G. Zhang, V.B.C. Tan, Y. Cheng, J.M. Bell, Y.-W. Zhang, Y. Gu, From brittle to ductile: a structure dependent ductility of diamond nanothread, Nanoscale 8 (2016) 11177–11184.
[45] H. Xie, F. Yin, T. Yu, J.-T. Wang, C. Liang, Mechanism for direct graphite-to-diamond phase transition, Sci. Rep. 4 (2014) 5930.
[46] C. Androulidakis, E.N. Koukaras, G. Paterakis, G. Trakakis, C. Galiotis, Tunable macroscale structural superlubricity in two-layer graphene via strain engineering, Nat. Commun. 11 (2020) 1–11.
[47] R.J. Swenson, Comments on virial theorems for bounded systems, Am. J. Phys. 51 (1983) 940–942.
[48] D.H. Tsai, The virial theorem and stress calculation in molecular dynamics, J. Chem. Phys. 70 (1979) 1375–1382.
[49] T.-B. Ma, L.-F. Wang, Y.-Z. Hu, X. Li, H. Wang, A shear localization mechanism for lubricity of amorphous carbon materials, Sci. Rep. 4 (2014) 3662.
[50] A. Stukowski, Visualization and analysis of atomistic simulation data with OVITO–the Open Visualization Tool, Model. Simulat. Mater. Sci. Eng. 18 (2009) 15012.
[51] V.I. Levitas, D.L. Preston, Three-dimensional Landau theory for multivariant stress-induced martensitic phase transformations. I. Austenite↔ martensite, Phys. Rev. B 66 (2002) 134206.
[52] Y. Peng, L. Xiong, Atomistic computational analysis of the loading orientation-dependent phase transformation in graphite under compression, JOM 71 (2019) 3892–3902.